Tunnelling and Underground Space Technology 67 (2017) 132–146

Contents lists available at ScienceDirect

Tunnelling and Underground Space Technology

journal homepage: www.elsevier.com/locate/tust

The long-term safety of a deeply buried soft rock tunnel lining under inside-to-outside seepage conditions

Fanjie Yang[a,b], Chuanqing Zhang[a,b,*], Hui Zhou[a,b], Ning Liu[c], Yang Zhang[c], Muhammad Usman Azhar[a,b], Feng Dai[d]

[a] State Key Laboratory of Geomechanics and Geotechnical Engineering, Institute of Rock and Soil Mechanics, Chinese Academy of Sciences, Wuhan, Hubei 430071, China
[b] University of Chinese Academy of Sciences, Beijing 100049, China
[c] HydroChina Huadong Engineering Corporation, Hangzhou, Zhejiang 310014, China
[d] State Key Laboratory of Hydraulics and Mountain River Engineering, Sichuan University, Chengdu, Sichuan 610065, China

ARTICLE INFO

Keywords:
Deep tunnel
High geostress
Time-dependent deformation
Lining safety
Seepage

ABSTRACT

For deeply-buried long tunnels, which are constructed in environments with high stress and soft rock, stability is definitely an important engineering problem. In this study, the buried depth of the chlorite schist section of a headrace tunnel in the Jinping II Hydropower Station was between 1550 and 1850 m. In this project, rheological problem, the wetting-induced softening problem and inside-to-outside seepage problem were all prominent, which posed serious threats to the long-term stability of the tunnel lining. This study detailed inspected the engineering geological conditions of the chlorite schist sections, the extrusion deformations of the surrounding rock mass following the excavation, and the surrounding rock support and reinforcement after the expansion excavations. In addition, the characteristics of rheological mechanical and wetting-induced softening for the chlorite schist were determined through laboratory testing and field monitoring. The rheological mechanical characteristics of the chlorite schist were not obvious when the stress was low. However, they were quite obvious when the stress was high. Based on the results, the rheological mechanical behaviors of the chlorite schist were described by a visco-elastoplastic rheological model (CVISC). Then, this study verified the rationality of the existing reinforcement scheme and obtained the final deformation stability time of the surrounding rock through a numerical simulation of the support reinforcement and the secondary lining during the operational period. Furthermore, the safety of the lining structure during the operational period was evaluated. These results may potentially play an important role in the guidance of future engineering designs and construction and may potentially be used as a reference for the support designs of similar deeply buried soft rock projects.

1. Introduction

Soft rock has the features of low strength, large deformations, serious wetting-induced softening, and obvious rheological effects (Liao et al., 2006; Sharifzadeh et al., 2013). In headrace tunnels, being excavated in deeply-buried soft rocks, the problem of deformation during the excavation and installation of supports is quite serious. And these problems along with their controlling factors will undoubtedly pose major threats to long-term safety of the tunnel lining during its operational period. For example: ① The long-term rheological deformation of the surrounding rock, which is under high stress, will constantly increase the lining pressure; ② During its operational period, the long-term inside-to-outside seepage will cause rock softening which can reduce the strength and deformation modulus, and leads to cracking and instability of the lining; ③ The cracking of the lining will speed up the seepage and softening of the surrounding rock (Tang and Tang, 2012; Zhao et al., 2015; Zhang et al., 2016). As a result, a vicious cycle will occur. For example, the chlorite schist of the Jinping II Hydropower Station exhibited the characteristic of a typical soft rock. After the excavation and support of the upper section, extrusion deformations of the surrounding rock appeared within a short time and became worse as further time elapsed. If these problems are not addressed during the construction period, the maintenance cost and power generation loss will become incalculable when cracks and damages occur to the lining due to the extrusion deformations of the surrounding rock. Therefore, stability of tunnels in deeply-buried soft rock and tunnel lining both are key controlling factors in the long-term safety of deep tunnel engineering projects.

* Corresponding author at: State Key Laboratory of Geomechanics and Geotechnical Engineering, Institute of Rock and Soil Mechanics, Chinese Academy of Sciences, Wuhan 430071, China.
E-mail address: cqzhang@whrsm.ac.cn (C. Zhang).

http://dx.doi.org/10.1016/j.tust.2017.05.004
Received 27 October 2016; Received in revised form 25 March 2017; Accepted 4 May 2017

Many researchers have carried out in-depth studies regarding soft rock engineering. By considering mechanical properties of weak rocks, Yoshida et al. (1997) calculated and analyzed the weakening of mudstone due to absorption of water and its influence on mechanical behavior of surrounding rock mass in tunnels. Mechanical response of surrounding rock mass during the excavation of rounded tunnel in viscoelastic media under hydrostatic pressure was studied by Fahimifar et al. (2010). Sulem et al. (1987) calculated and analyzed the rheological mechanical laws of the surrounding rock in rounded soft rock tunnels using an empirical formula. Guan et al. (2008) used Burger-deterioration rheological model to calculate and analyze the surrounding rock deformation in a mountainous tunnel. Pellet et al. (2009) adopted a numerical simulation method to calculate the rheological mechanical behaviors of the damage zones in surrounding rock mass following the excavations of underground galleries. By considering support in soft rock tunnels, Sakurai (1978) deeply examined stresses and support structures during the excavation of tunnels. Carranza and Diederichs (2009) calculated and analyzed the mechanical behavior of wire mesh and shotcrete composite lining in rounded tunnels. Creep characteristics of galleries in soft surrounding rock mass with bolt-grout supports were studied by Lian et al. (2008) by numerical simulation. Pellet (2009) studied the contacts between the tunnel lining in viscoelastic media and the surrounding rock within easily damaged areas. He et al. (2015) applied the material point method to evaluate the safety of excessive deformations in tunnels.

In deeply-buried soft rock tunnel engineering, it is necessary to consider following three factors: rheology of the rock mass, inside-to-outside seepage (Zarei et al., 2012, 2013) and wetting induced softening. These factors play a vital role in the safety of tunnels in deeply-buried soft rock masses because of the complex physical and mechanical properties of soft rocks, unfavorable geological environment and engineering conditions. The lining structure stresses, which arise from the rheological and elastic-plastic deformations of the surrounding rock mass, are the loading conditions that require consideration during the analysis of lining design and safety. The combined action of these factors is quite complicated because these are interconnected with each other. Therefore, research conducted on only a single factor cannot possibly meet the necessary requirements.

A chlorite schist formation was found during the excavation of a headrace tunnel at the Jinping II Hydropower Station. The formation had a total length of approximately 400 m, a burial depth of about 1550–1850 m, and gravity stress of approximately 42–50 MPa (Liu et al., 2013). After the tunnel excavation and initial support, the extrusion deformation became serious. The rheological effect was prominent, the wetting-induced softening effect was strong, and inside-to-outside seepage problem was existed. The aims of this study were to analyze and evaluate the lining structure safety during the operational period, based on a detailed inspection of the geological conditions, excavation method, initial support, and support reinforcement for the chlorite schist section. The processes of actual tunnel construction and tunnel operational conditions were analyzed using visco-elastic rheological model. The rheology mechanical behavior of the rock mass and the wetting-induced softening effect were also considered in this analysis. The fluid-solid coupling method was applied in this analysis. Then, several indexes, including the rheological deformation, stress, FAI (Failure Approach Index (Zhang et al., 2011), which is an index for the strain assessment) and plastic zone, were introduced to evaluate the safety of the surrounding rock mass and lining structure. Fig. 1 illustrates the flow chart of the research work in this paper.

2. Engineering situations of the chlorite schist section in the Jinping II Hydropower Station

2.1. Engineering geological characteristics of the chlorite schist section

The headrace tunnel of the Jinping II Hydropower Station consisted of four parallel headrace tunnels, with a total length between 16.658 and 16.675 km, maximum burial depth 2525 m, and average burial depth approximately 1610 m. The chlorite schist of the Jinping II Hydropower Station was mainly distributed in K1 + 537 to K1 + 800 of the #1 headrace tunnel, and K1 + 613 to K1 + 755 of the #2 headrace tunnel. It had a burial depth ranging from 1550 m to 1850 m and gravity stress value approximately 41–50 MPa. The majority of the surrounding rocks were grade-IV (Ministry of Water Resources of the People's Republic of China, 2008), as shown in Fig. 2.

The strata, which were exposed during the excavation of the west end of the headrace tunnels, mainly consist of lower Triassic green schist (T_1), middle Triassic Zagunao Formation marble (T_{2z}), and lower Triassic sand slate (T_3). The T_1 was interbedded and consisted of green sandstone, chlorite schist, and gray white/light fresh pink marble with each layer thickness between 20 cm and 60 cm. The attitude change of the chlorite schist was quite large, with a strike of NS SN to N 20° E, an inclination direction of W/NW, and an inclination angle of ∠75° to 85°. The chlorite schist stratum constitute the core of an anticline with T_{2Z} in conformal contact on both sides as shown in Fig. 2. For the lithology boundary, the strike is N28° to N45°, the inclination direction is W/NE, and the inclination angle is 55°. The attitude of the strata in the K1 + 200 to K1 + 900 m section was found to be very complex, and changed from NE (intersected with the tunnel axis at a large angle) to NW (parallel to the tunnel axis). There were many complex folds observed in this section due to which the rocks were strongly extruded, distorted, and crumpled. After the extrusion of chlorite schist from the tunnel, the surrounding rocks became so weak and loose that they can be broken off by hand. There was no big adverse structural plane through the chlorite schist section. The gaps between the small structural planes were filled with rock flour and thereby the small structural planes were smooth. The chlorite schist formation acted as a water-resistant layer which ceases the further growth of karst and movement of underground water. Therefore, the external water action could be neglected during the design of the lining structure.

2.2. Excavation support of the chlorite schist section

In accordance with the lithology classification and surrounding rock quality, the tunnel diameters and support parameters during the initial excavation were shown in Tables 1 and 2. In this project, rock mass basic quality [BQ] system (Ministry of Housing and Urban-Rural Development of the People's Republic of China, 2015) was applied for evaluation of rock mass quality. It is the engineering rock mass classification standard of China (GB/T50218-2014), in which rock mass quality could be divided into five grades by the [BQ] value ($[BQ] \in [550, +\infty]$, Grade I; $[BQ] \in [550, 451]$, Grade II; $[BQ] \in [450, 351]$, Grade III; $[BQ] \in [350, 251]$, Grade IV; $[BQ] \in (-\infty, 250]$, Grade V). For the chlorite schist in the Jinping II hydropower station, the [BQ] value was 286 and the quality of chlorite schist belongs to grade IV. The design tunnel diameter was between 13.4 and 13.8 m. Top heading and benching method was used to excavate the tunnel with upper bench height was 8.5 m and lower bench height was between 4.9 m and 5.3 m. The excavation was divided into left and right parts, and a steel arch grid was erected following the excavation of the upper bench. Soon after, anchor bolts were installed and shotcreting was done as initial support for the tunnel. In addition, steel fiber-reinforced siliceous concrete with outstanding bending resistance was adopted. The majority of the anchor bolts were full-length common mortar anchor bolts.

Support parameters listed in Tables 1 and 2 are:

- *S4-n:* The tunnel diameter was 13.4 m; diameters of the systematic bolts in the full-section were 28–32 mm; the lengths of the anchor bolts were 6–9 m, which were alternatively arranged with 1-m spacing; the thickness of the steel fiber-reinforced siliceous concrete was 20 cm; the spacing between the grid steel arch was 1.0 m;

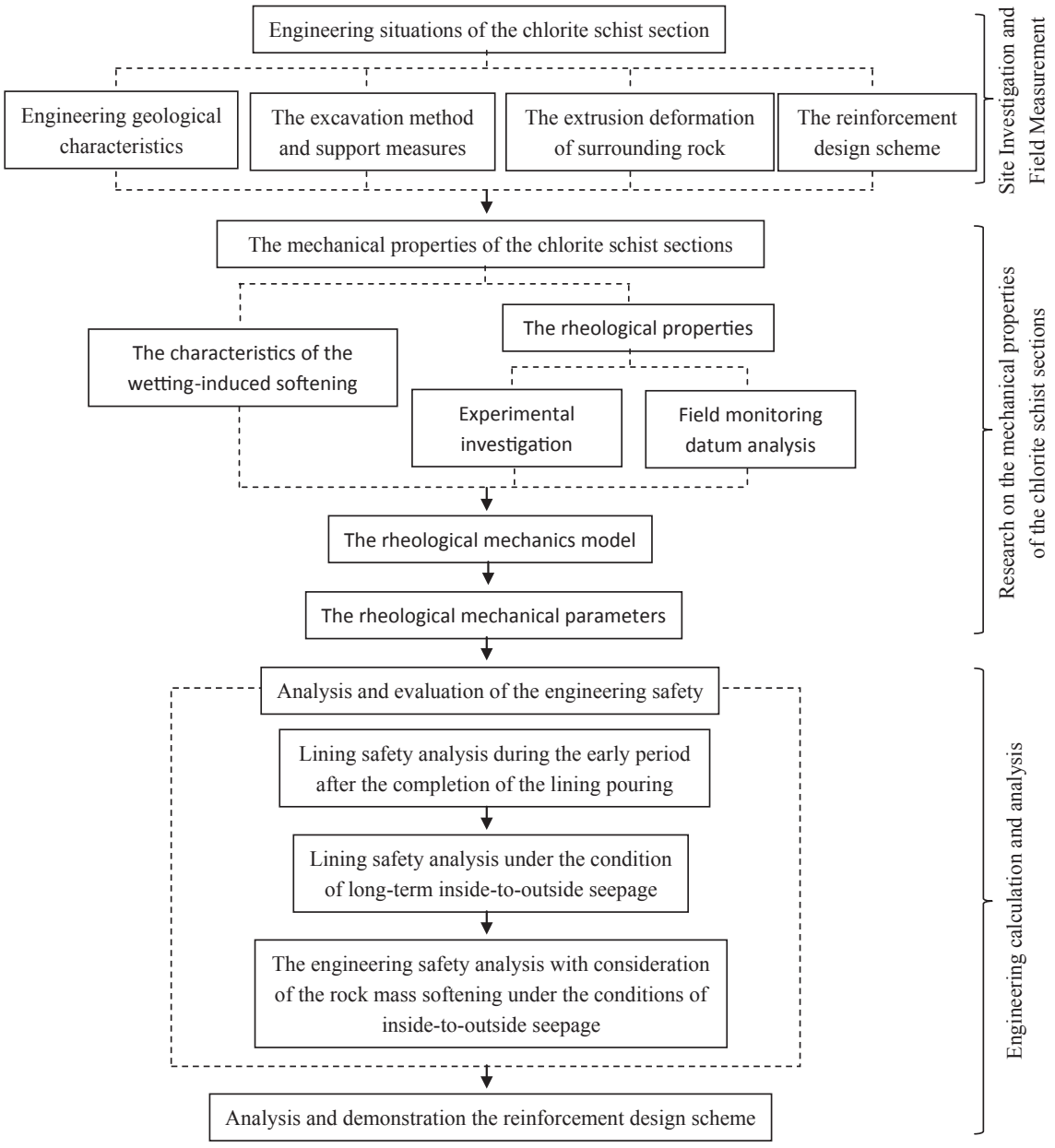

Fig. 1. The flow chart of the research work.

advanced self-drilling hollow grouting anchors were installed within a 120° scope of the arch crown, with diameter of 28–32 mm, or small ducts with diameters between 42 and 45 mm, lengths of 4.5 m, and with 0.6-m spacing.

- *S8:* The tunnel diameter was 13.4 m; the diameter of the systematic bolts in the full-section was 32 mm; the lengths of the anchor bolts were 9 m, alternatively arranged with 1-m spacing; the thickness of the steel fiber-reinforced siliceous concrete was 20 cm; the spacing between the grid steel arch was 1.0 m; advanced self-drilling hollow grouting anchors were installed within a 120° scope of the arch crown, with diameters between of 28 and 32 mm, or small ducts with diameters of 42–45 mm, lengths of 4.5 m, and with 0.6-m spacing.
- *S8-n:* The tunnel diameter was 13.8 m; the diameters of the systematic bolts in the full-section were 28–32 mm; the lengths of the anchor bolts were between 6 and 9 m, alternatively arranged with 1-m spacing; the thickness of the steel fiber-reinforced siliceous concrete was 20 cm; the spacing between the grid steel arch was 0.5 m; advanced self-drilling hollow grouting anchors were installed within a 120° scope of the arch crown, with diameters between 28 and 32 mm, or small ducts with diameters of 42 and 45 mm, lengths of 4.5 m, and 0.3-m spacing; the excavation footage was within 1 m; 10-cm-thick steel fiber-reinforced siliceous concrete was sprayed into the tunnel face for a timely closure.
- *S8-n′:* The tunnel diameter was 13.8 m; a row of advanced anchor bolts (anchor piles) or advanced small ducts were installed within a 150° scope of the arch crown, with a circumferential spacing of 30–40 cm, and an external angle of 5–10°; two rows were installed in the sections where collapse may have easily occurred; following the excavation, 5- to 10-cm-thick steel fiber-reinforced siliceous concrete was sprayed into the tunnel face for closure, according to the surrounding rock's crushing degree; if the tunnel face was unstable, random fiberglass anchor bolts were installed, with diameters of 25 mm, and lengths of 4.5 m; 5- to 8-cm-thick steel fiber-reinforced siliceous concrete was sprayed into the tunnel face during the initial stage, and steel mesh with a diameter of 8 mm and grid spacing of 15 cm × 15 cm was hung; a grid arch (or section steel arch) with a longitudinal spacing of 0.5–1.0 m was installed,

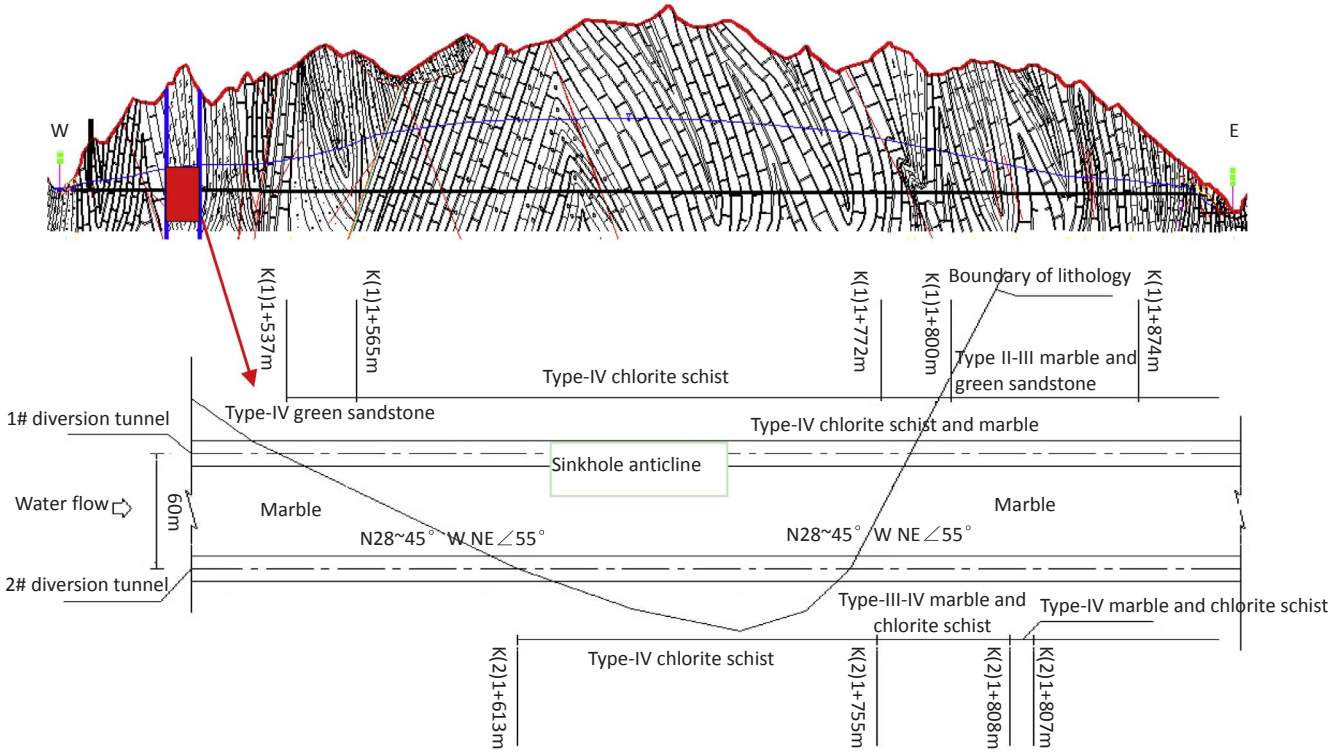

Fig. 2. Engineering geological conditions of the chlorite schist section of the Jinping II Hydropower Station (Liu et al., 2013).

and systematic bolts with diameters of 32 mm, lengths between 6 and 9 m, and spacing of 1.0 m were used. Then, 25–30 cm of thick steel fiber-reinforced siliceous concrete was sprayed, and the excavation footage was within 1 m.

2.3. The extrusion deformation of the chlorite schist section

The dominant failure type of surrounding rock mass was considered as plastic shear failure under high stress due to low strength of chlorite schist, with a concrete form of large deformations (mainly referring to the plastic deformations). During the excavation of the upper bench, serious extrusion deformation occurred in the chlorite schist section. The maximum deformations in the chlorite schist sections of the #1 and #2 tunnels are shown in Figs. 2 and 3, respectively. According to statistical analysis, in tunnel #1, the maximum deformation covered approximately 51% of the section and exceeded 0.5 m; 74.6% of the section displayed serious or extremely serious extrusion deformations; 23.08% of the section displayed moderate extrusion deformation; and the remaining section displayed slightly extrusion deformation. In tunnel #2, the maximum deformation covered more than 30% of the section and exceeded 0.5 m; 58.93% of the section displayed serious or extremely serious extrusion deformation, and 36.5% of the section displayed moderate extrusion deformation. Therefore, the extrusion deformation of the tunnel #1 is more serious than the tunnel #2. In additional, the range of K1 + 710–720 in tunnel #1 is the most unfavorable position from Fig. 3, with larger deformation of surrounding rock. And, the engineering geological of the range is typical type-IV chlorite schist. So, the K1 + 715 section was selected as the critical section for next research.

A comparison of the tunnel sections before and after the expansion excavation is shown in Fig. 4(a) and (b), which intuitively reflect the degrees of the extrusion deformation. Due to the lack of a locking treatment for the skewback after the upper bench excavation, and the failure that occurred during the timely drainage of water, the rock mass in the skewback softened when it became wet, and the deformation in the skewback was found to be the most serious, as shown in Fig. 5(b).

2.4. The reinforcement design scheme of the chlorite schist section

In order to guarantee the section area in the cross section and the stability of the tunnel during the lower bench excavation, the designer and investor decided to carry out expanding excavation and to adopt support reinforcements for the expansion excavation section. A rock drill was adopted for the expanding excavation. The expansion excavation was gradually carried out with a steel arch spacing (the spacing are dependent upon the support types) as the step pitch and with timely closures and support for the sections following the expansion excavations, as shown in Fig. 5. The parameters of the section support reinforcements following the expansion excavation are shown in Fig. 6, which include the installation of advanced anchor piles (32-

Table 1
Support design of the chlorite schist section in diversion tunnel #1.

Stake no. (m)	Section length (m)	Lithology	Type of surrounding rock	Tunnel diameter (m)	Support type
1+537–565	28	Green sandstone	IV	13.4	S4-n
1+565–618	53	Chlorite schist	IV	13.4	S4-n
1+618–662	44	Chlorite schist	IV	13.4	S8
1+662–760	98	Chlorite schist	IV	13.8	S8-n
1+760–772	12	Chlorite schist	IV	13.8	S8-n′
1+772–800	28	Chlorite schist, interbedded marble, and chlorite schist	IV	13.8	S8-n’

Table 2
Support design of the chlorite schist section in diversion tunnel #2.

Stake no. (m)	Section length (m)	Lithology	Type of surrounding rock	Tunnel diameter (m)	Support type
1 + 613–643	30	Chlorite schist	IV	13.4	S8
1 + 643–672	29	Chlorite schist	IV	13.8	S8-n′
1 + 672–745	73	Chlorite schist, interbedded chlorite schist, and marble in partial area	IV	13.8	S8-n′
1 + 745–755	10	Marble and chlorite schist in west side wall	IV	13.8	S8-n′

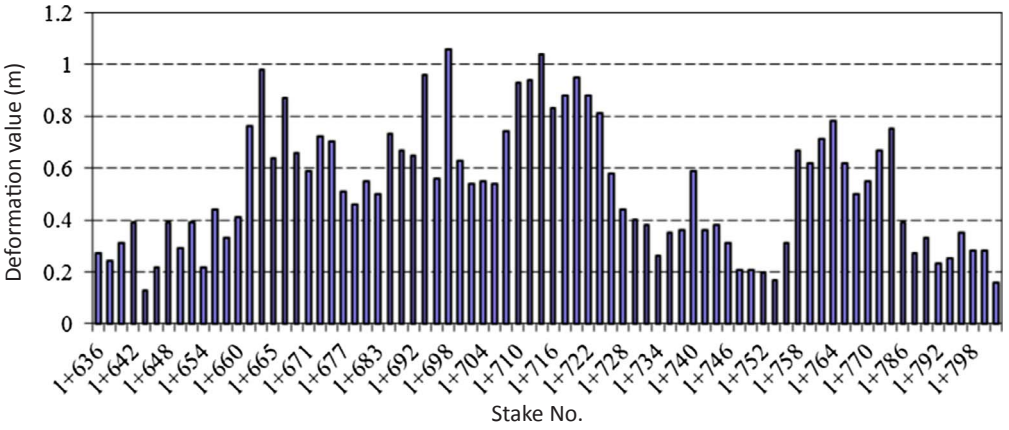

Fig. 3. Laser scanning of the surrounding rock deformation in the K1 + 635 and K1 + 800 sections of tunnel #1.

mm-diameter steel bars bound together) in the skewback, with a spacing of 1.0 m and length of 9 m. In addition, 32-mm-diameter pre-stressed anchor bolts were installed in the middle parts of the side walls, with a pre-stress of 150 kN, a spacing of 1.5 m and length of 9 m. Then, 32-mm-diameter common mortar anchor bolts were installed in the spandrel, with a spacing of 0.5 m and length of 9 m. Finally, two rows of 32-mm-diameter common mortar anchor bolts were installed in the lower parts of the side walls, with a spacing of 0.5 m or 1.0 m and length of 9 m. If the surrounding rock deformation rate or value was too large during the bottom excavation (for example, the deformation rate exceeded 10 mm/d for three consecutive days, or the accumulative deformation value exceeded 6 cm), then the pre-stressed anchor bolts were replaced with pre-stressed anchor cables in the middle parts of the side walls, with a pre-stress value of 1000 KN, a spacing of 3 m and length of 15 m.

The deformation in the surrounding rock was well-controlled after expansion excavation and support reinforcement, the deformation of surrounding rock mass, as shown in Fig. 7. However, a time-dependent transformation effect was still existed, and the effects of wetting-induced softening due to inside-to-outside seepage during the operational period was also developed over time. The safety of the lining structure was still threatened by the surrounding rock deformations. Therefore, it was considered necessary to analyze the safety of lining by taking time effect into account, as well as the effects of the wetting-induced softening, based on the conditions of excavation and support during the construction period.

3. Effects of the wetting-induced softening and the rheological characteristics of the chlorite schist

In this study, the mechanical engineering characteristics of the chlorite schist, the deformation strength characteristics, effects of the wetting-induced softening, and the rheological mechanical characteristics were examined through uniaxial, tri-axial, and rheological testing.

3.1. Deformation and strength characteristics and the effect of the wetting-induced softening

RMT 150C in housed testing machine with load control capability was used to conduct uniaxial compression test on chlorite schist

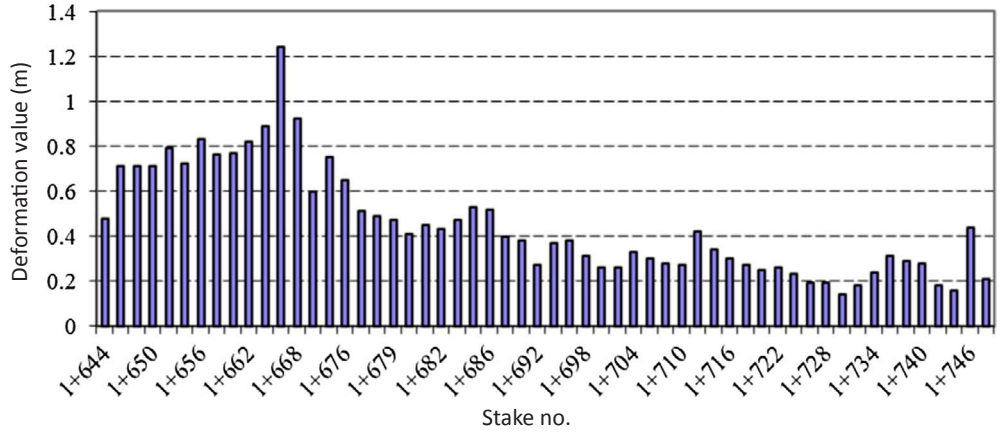

Fig. 4. Laser scanning of the surrounding rock deformations in the K1 + 643 and K1 + 748 sections of tunnel #2.

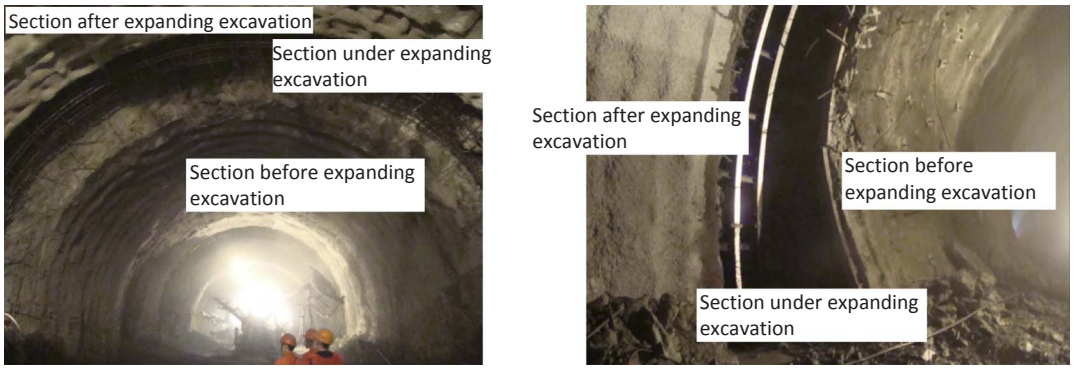

Fig. 5. Expanding excavation scene in the chlorite schist extrusion deformation section: (a) arch crown; (b) skewback.

samples under dry and saturated conditions. Before testing, the samples were dried using the oven drying method and then saturated by the vacuum pumping method. According to the uniaxial compression test results, the average elastic modulus of the chlorite schist was found to be 13.18 GPa under dry conditions and 3.54 GPa under saturated conditions, which is 27% of the former. The compressive strength of the chlorite schist was determined to be 38.8 MPa under dry conditions and 19.47 MPa under saturated conditions, which is almost 50% of the former. The study defined the ratio of the elastic modulus or the strength under saturated conditions to the corresponding value under dry conditions, as the elastic modulus softening coefficient or strength softening coefficient. The elastic modulus softening coefficient of the chlorite schist obtained in the uniaxial test was 0.27, and the strength softening coefficient was 0.5, both of which were relatively small. Therefore, the effect of the wetting-induced softening was quite prominent.

Furthermore, triaxial compression test was also carried out for chlorite schist samples under dry and saturated conditions by MTS815.03 testing instrument. According to the test results, the strength and elastic modulus softening coefficients under low confining pressure were relatively low, 0.45 and 0.14, respectively. The effect of the wetting-induced softening was obvious and decreased with increasing confining pressure. These results suggested that the confining pressure played an active role in inhibiting the effect of wetting-induced softening, as shown in Fig. 7(a) and (b) Zhou et al., 2014. In fact, the effect of confining pressure becomes more prominent due to the reduction in coefficient of permeability, which arises from the compaction effect at high confining pressures (see Fig. 8).

3.2. The rheological properties of the chlorite schist

3.2.1. Rheological deformation characteristics investigated by laboratory testing

This study developed uniaxial and triaxial rheological tests aiming the determination of rheological mechanical characteristics of chlorite schist. The axial loads under the uniaxial conditions were determined to be 4 MPa, 8 MPa, and 12 MPa. The axial loads under the tri-axial conditions were determined to be between 20 and 55 MPa. The rheological deformation curves of the chlorite schist under the different confining pressures are shown in Fig. 9. When the stress was low, the creep deformation was small, and the rheological characteristics were not obvious. However, when the stress was high, the rheological

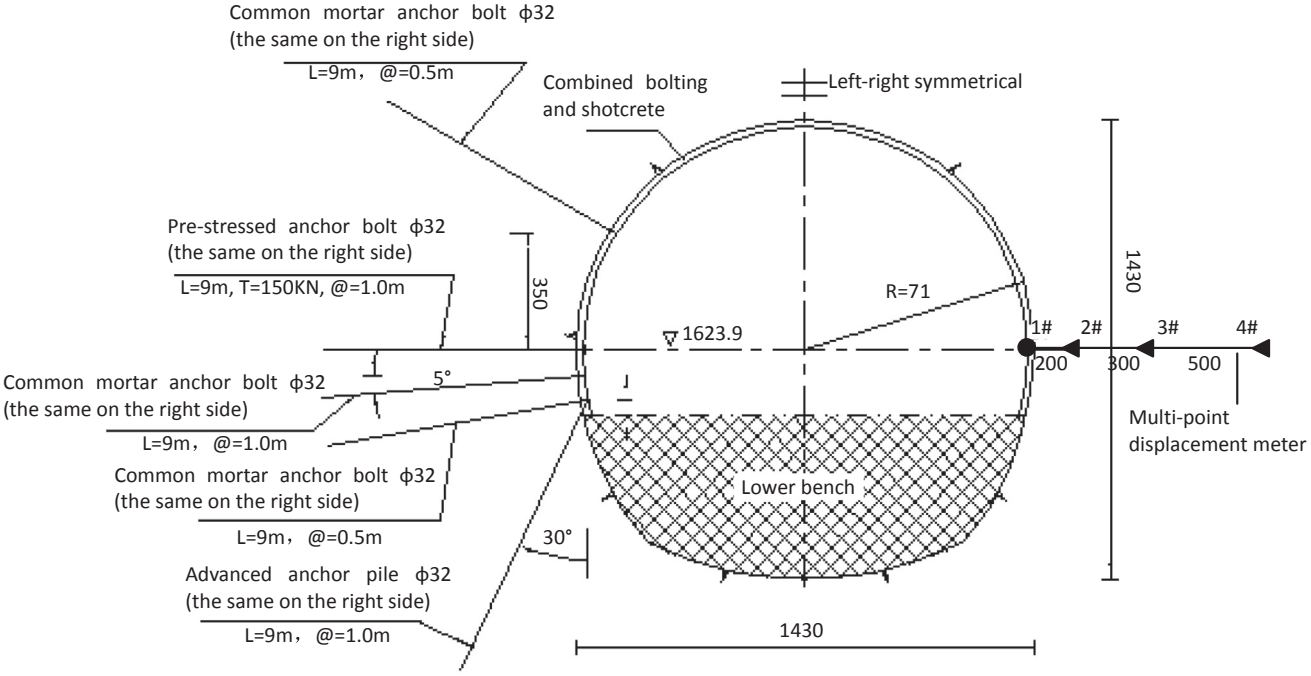

Fig. 6. Support reinforcement scheme and displacement monitoring layout of the chlorite schist section (cm). Φ: diameter; L: length; @: spacing; T: pre-stress; R: tunnel radius; ▽: elevation;

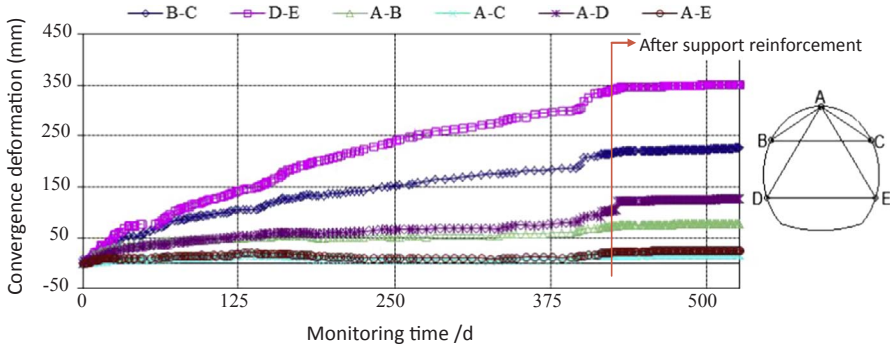

Fig. 7. Convergence deformation curve of the surrounding rock in the K1 + 780 section of tunnel #1.

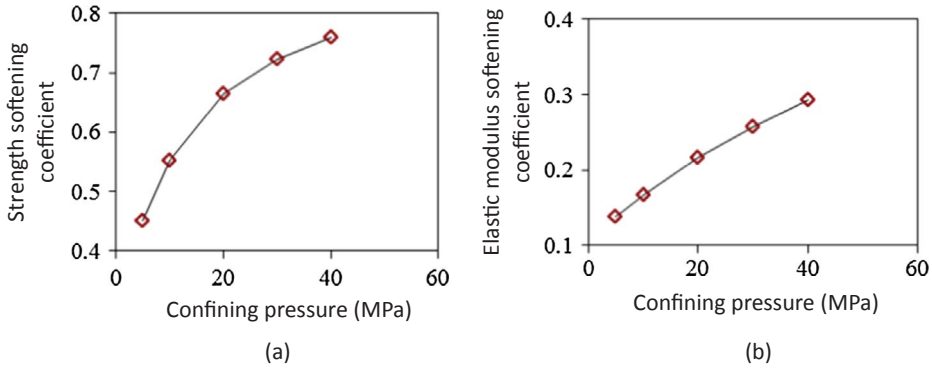

Fig. 8. Correlation between the elastic modulus and strength softening coefficient and the confining pressure (Zhou et al., 2014).

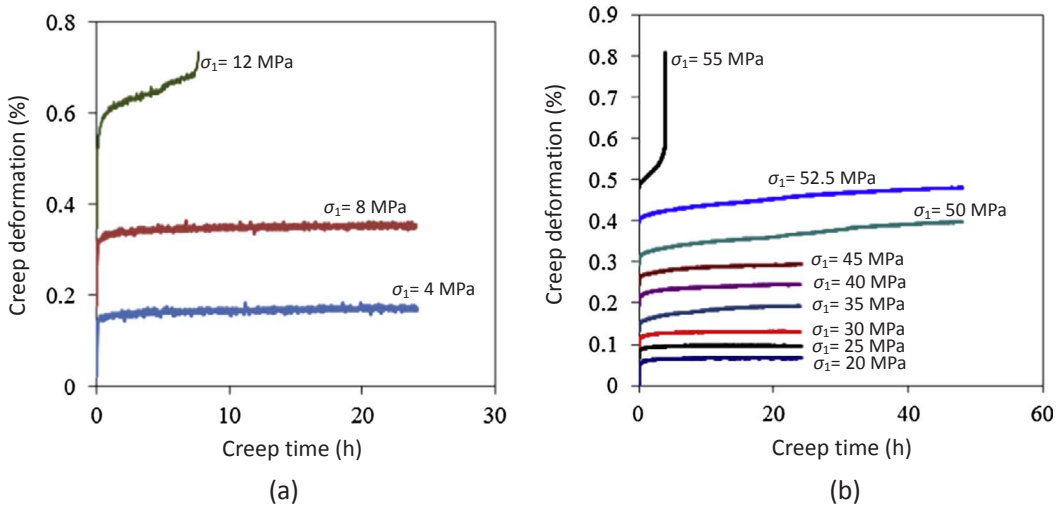

Fig. 9. Rheological deformation curve of the chlorite schist under different confining pressures: (a) σ_3 = 0 MPa; (b) σ_3 = 10 MPa.

characteristics were quite prominent. Under the uniaxial conditions, the rheological characteristics were obvious when the load was above 8 MPa, and the load was above 35 MPa when the confining pressure was 10 MPa, or approximately 65% of the long-term strength. From the stable creep to the accelerated creep an obvious transition phase was observed while the strength being close to the long-term value.

3.2.2. Rheological deformation characteristics reflected by the field monitoring curve

The rheological test results only showed the mechanical behavior of a complete rock block, but they could not fully reflect the mechanical properties of rock masses with complex structures and components. Therefore, to study long-term deformation in surrounding rock mass, field monitoring using multi-point displacement meter was adopted, in order to directly show the rheological characteristics of the rock mass.

After the expansion excavations and support reinforcements of the chlorite schist section in the Jinping II Hydropower Station, a multi-point displacement meter was used to monitor the K1 + 715 section in tunnel #1. The monitoring layout diagram is shown in Fig. 6. Total four monitoring points were selected and the corresponding surrounding rock deformation monitoring curves are shown in Fig. 10. The stress adjustment and deformation of the surrounding rock occurred during the excavation of the left section of the lower bench, and the deformation did not stop after the excavation was completed. At the 100-day point, the displacement value reached approximately 9 mm. The excavation of right section of the lower bench was started after 180 days when the displacement value was 12.3 mm. The deformation of surrounding rock mass increased during the excavation and con-

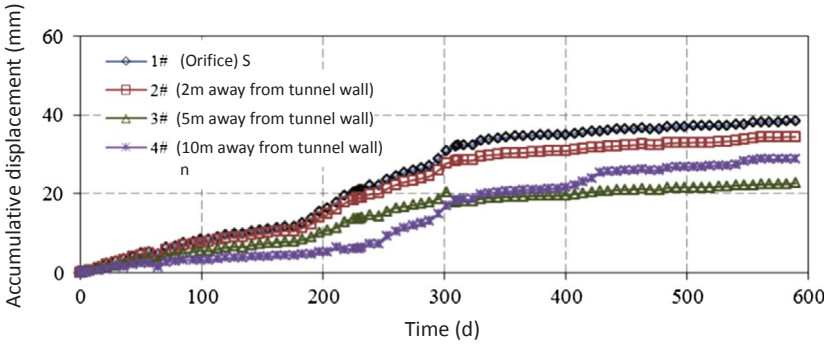

Fig. 10. Displacement monitoring curve in the K1 + 715 section of tunnel #1.

tinued to increase after the excavation was completed. The displacement value reached 32.9 mm on the 320th day, after which the deformation increment decreased and the displacement value was 37.4 mm on the 540th day. As can be seen in Fig. 10, the displacement value at 10 m away from tunnel wall was larger than the surrounding rock deformation at 5 m. This may have been caused by a partial geological structure. However, the site analysis failed to reveal the partial geological structure. Therefore, it could not be used as basic data in the subsequent analysis of this study.

According to the field monitoring results, the stress level of the surrounding rock following the excavation exceeded the level that emerged from the obvious rheological deformations in the test. Therefore, during long-term stability analysis it was necessary to consider the rheological mechanical behavior of the surrounding rocks.

4. Selection of the rheological mechanics model for the chlorite schist and the inverse analysis of the mechanical parameters

4.1. Selection of the rheological mechanics model

As previously detailed, the chlorite schist had an obvious rheological property, and in the later rheological stage, specimens develop great plastic deformation when subjected to high-stress conditions, which finally leads to the failure of the specimens. In other words, the plastic and viscous flows coexisted. Therefore, future modeling of the rheological mechanical behavior of the chlorite schist must consider the plastic deformation behavior of rock masses.

As can be seen in Figs. 9 and 10, the creep deformation of the chlorite schist gradually increased with time. However, when the stress was lower than the creep's long-term strength, the creep deformation rate decreased with time, and it tended to be the limit having a stable value. For example, there was a horizontal asymptote on the curve, and this rheological behavior belonged to the Maxwell-type rheology. Meanwhile, under the different stress levels, the rheological curve of the chlorite schist displayed similar convergence and divergence, and thus the chlorite schist also had Kelvin-type rheological behavior. Therefore, the rheological mechanical behavior of the chlorite schist could be described by using the Burgers rheological model, which integrates the characteristics of the Maxwell and Kelvin models. In combination with the existing research results (Pellet et al., 2009; Pellet, 2009; Bonini et al., 2009), this study used a visco-elastoplastic rheological mechanical model (CVISC) to describe the rheological mechanical behavior of the chlorite schist.

Sharifzadeh et al. (2013) introduced the visco-elastoplastic rheological mechanical model (CVISC) in FLAC^{3D} software. This model consists of the Burgers rheological component and the Mohr-Coulomb friction component, as shown in Fig. 11. In this model, the total deviatoric stain rate was obtained using Formula (1), where the component of each deviatoric stain rate can be calculated using Formulas (2)(4). The elastic-plastic volumetric stress mechanics behavior is indicated in Formula (5). In this formula, the superscript *Ke, M,* and *P* represent the corresponding components of the Kelvin, Maxwell, and MC plasticity respectively; K and G represent the bulk modulus and shear modulus, respectively; g is the dynamic coefficient of the viscosity; e_{ij} and S_{ij} represent the deviatoric stain tensor and deviatoric stress tensor, respectively; e_{vol} and σ_0 represent the volumetric strain tensor and volumetric stress tensor, respectively; and $\lambda\star$ represents the plastic factor.

$$\dot{e}_{ij} = \dot{e}_{ij}^{Ke} + \dot{e}_{ij}^{M} + \dot{e}_{ij}^{P} \tag{1}$$

$$S_{ij} = 2\eta^{Ke}\dot{e}_{ij}^{Ke} + 2G^{Ke}\dot{e}_{ij}^{Ke} \tag{2}$$

$$\dot{e}_{ij}^{M} = \frac{\dot{S}_{ij}}{2G^{M}} + \frac{S_{ij}}{2\eta^{M}} \tag{3}$$

$$\dot{e}_{ij}^{P} = \lambda^{*}\frac{\partial g}{\partial \sigma_{ij}} - \frac{1}{3}\dot{e}_{vol}^{P}\delta_{ij}, \quad \dot{e}_{vol}^{P} = \lambda^{*}\left[\frac{\partial g}{\partial \sigma_{11}} + \frac{\partial g}{\partial \sigma_{22}} + \frac{\partial g}{\partial \sigma_{33}}\right] \tag{4}$$

$$\dot{\sigma}_0 = K\left(\dot{e}_{vol} - \dot{e}_{vol}^{P}\right) \tag{5}$$

With regards to the Mohr-Coulomb criterion, the yield criterion and potential function are shown in Formulas (6) and (7), respectively.

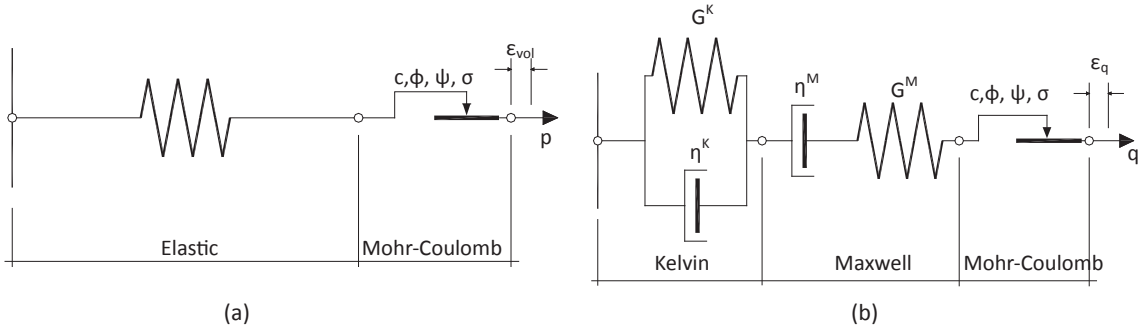

Fig. 11. Schematic representation of the CVISC model: (a) volumetric behavior; and (b) deviatoric behavior (Sharifzadeh et al., 2013).

$$f = \sigma_1 - \sigma_3 \frac{1+\sin\phi}{1-\sin\phi} + 2c\sqrt{\frac{1+\sin\phi}{1-\sin\phi}} \tag{6}$$

$$g = \sigma_1 - \sigma_3 \frac{1+\sin\psi}{1-\sin\psi} \tag{7}$$

where σ_1 and σ_3 represent the maximum and minimum principal stresses, respectively, while c, φ, and ψ represent the cohesion, internal friction angle, and dilatancy angle, respectively.

In this study, it was found that the CVISC rheological mechanics model was not only able to comprehensively reflect the rheological and plastic mechanics behavior of the rock mass but was also simple to deal with. However, there was an uncertainty as to whether it could describe the mechanical behavior of the chlorite schist rock mass. Therefore, this study still needed to conduct a comparison evaluation with the mechanical response of the surrounding in situ rocks.

4.2. Inversion of the rheological mechanics parameters

For the purpose of evaluating the applicability of the CVISC mechanics model, determining the mechanical parameters of surrounding rock, and laying a foundation for the subsequent engineering analysis, parameter inversion was performed, as well as the calculation of the mechanical response of the surrounding rock, on the basis of the monitoring data, which are shown in Fig. 10.

The calculations for the chlorite schist section of the tunnel were carried out using the CVISC mechanics model. The simulation time of the rheology was 400 days after the lining of the tunnel was implemented. Since the chlorite schist tunnel section in the Jinping II Hydropower Station was comparatively long along the tunnel axis, the issue could be dealt with easily by considering it to the plane strain issue. The grid model and related dimensions of the K1 + 715 cross-section in tunnel #1 are shown in Fig. 12. The model width and height were both 180 m; the upper bench excavation height in the tunnel was 8.5 m; and the radius of the upper cross-section was 7.15 m. The numerical model contained 9658 units and 19,438 nodes. The boundary condition of the model adopted a normal constraint, and the initial stress field was set as follows: σ_x = 32.8 MPa, σ_y = 39.2 MPa, σ_z = 37.6 MPa, and σ_{xz} = 2.8 MPa.

In order to simulate the actual construction sequence, the 8.5-m upper bench was first excavated, and the corresponding reinforcement measurements in the areas disturbed by the excavation of the upper bench were recorded (the selected reinforcement areas were approximately 9 m according to the site construction condition). Meanwhile, the observation points in the right haunch position were arranged with a specific monitoring location in order to monitor the deformation of the surrounding rock, as shown in Fig. 6. Afterwards, the excavation and lining of the lower bench was carried out.

Since the current numerical simulation technique had difficulty in simulating the supporting effect of the anchor rod, anchor rope, and anchor bar pile in the underground engineering, this study approximately simulated the effect after the reinforcement by changing the mechanical parameters of the rock mass in the supporting reinforcement area, thereby obtaining the mechanical parameter part of this area using an inversion method.

A displacement back-analysis method (Feng et al., 2016), which was based on particle swarm optimization (PSO), was used for the inversion of the CVISC parameters. This method adopted the FISH language in FLAC^{3D} to compile the parameter inversion program, which was based on the PSO optimization algorithm, and also embedded the FLAC^{3D} numerical calculation software for the purpose of the calculation. The specific implementation procedures were as follows:

(1) Initialize a particle swarm: for example, first initialize the location and speed of each particle randomly within a certain range of the interval and evenly distribute them in the solution space;
(2) Set the moderate degree function as follows:

$$F(x) = \sum_{i=1}^{n} [f_i(x) - u_i]^2 \tag{8}$$

where x is the parameter to be inverted; $f_i(x)$ is the calculated value of the displacement at the ith measurement point; u_i is the actual measured value of the displacement; and n is the total number of monitoring points;
(3) Substitute the calculation parameters and boundary conditions into FLAC^{3D} in order to calculate the fitness function value for each of the particles;
(4) On the basis of the fitness, select the optimum location (p_{id}) from the individual extremums experienced by each particle;
(5) On the basis of the fitness, select the optimum location (p_{gd}) of each particle from the global extremum experienced by the entire particle swarm;
(6) Change the moving speed and location of particles according to Formula (9):

$$\left.\begin{aligned} v_{id} &= w v_{id} + c_1 r_1 (p_{id} - x_{id}) + c_2 r_2 (p_{gd} - x_{id}) \\ x_{id} &= x_{id} + v_{id} \end{aligned}\right\} \tag{9}$$

where v_{id} is the speed of the ith particle in the dth dimension; x_{id} is the location of the ith particle in the dth dimension; r_1 and r_2 indicate the Uniform Random Number between (0,1); c_1 and c_2 represent the learning factor (in most cases, $c_1 = c_2$ taking the

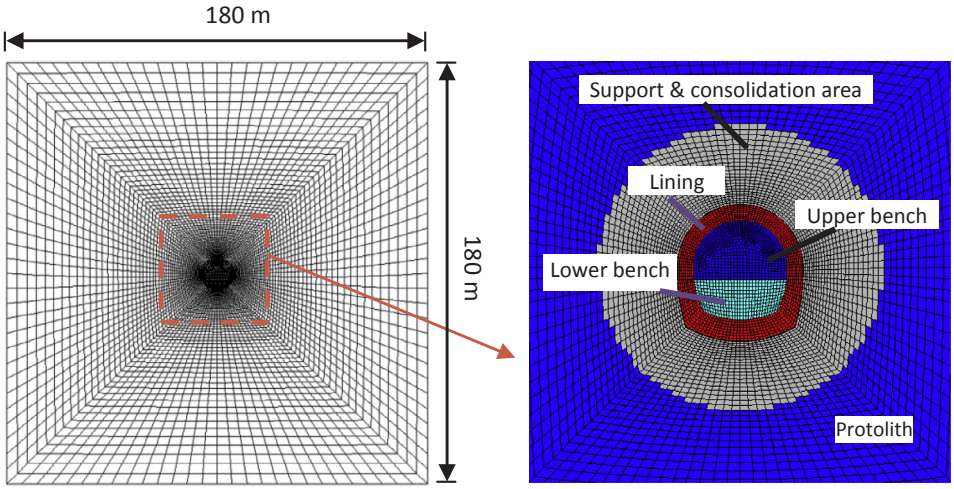

Fig. 12. Schematic diagram of the numerical calculation model.

Table 3
Value of the calculated parameters of the rheological mechanics model of the chlorite schist.

	Kelvin shear modulus G^{Ke} (GPa)	Kelvin viscosity coefficient η^{Ke} (GPa d)	Maxwell shear modulus G^{M} (GPa)	Maxwell viscosity coefficient η^{M} (GPa d)	Bulk modulus K (GPa)	Cohesion force c (MPa)	Internal friction angle ϕ (°)
Protolith	20.00	1.25e3	2.72	1.12e8	3.63	2.54	35.18
Support and consolidation area	20.00	1.25e3	1.70	1.00e8	2.27	2.06	31.69

value within (1.8–2.0)); and w is the inertia weight;

(7) If the termination condition is satisfied (which usually meant that the maximum number of iterations, and the optimum location searched by the particle swarm up to a set point met the fitness threshold), then stop the iteration, and output the optimum location of the particle. Otherwise, return to Step (3).

In the parameter inversion, the more parameters to be solved, the lower the reliability of the obtained parameter values. Hence, this study first determined the values of some of the parameters in accordance with the site test results and the empirical value, by implementing the method presented by Hoek for rock mass parameters. Then, the remaining parameters were inverted. The bulk modulus K and the Maxwell shear modulus G^{M} of the protolith and support and the reinforcement area of the chlorite schist were obtained in accordance with the test results of the elasticity modulus of the site borehole, as shown in Table 3. The cohesion c and internal friction angle ϕ of the protolith were determined on the basis of the empirical value using the Hoek method of rock mass parameters. For example, when the laboratory uniaxial compression strength of the chlorite schist was known, GSI = 66, mi = 10, and D = 0 were used to obtain the corresponding parameter values, as shown in the Table 3. The surrounding rock in the support and reinforcement areas was found to have been disturbed by the blasting operation during the construction and excavation processes and also suffered fractural damage resulting from the high stress. Therefore, the GSI value was lower (54) than that of the undisturbed protolith, while the corresponding c and ϕ values were as shown in Table 3. The Kelvin shear modulus G^{Ke} and the Kelvin viscosity coefficient η^{Ke} in the respective protolith and reinforcement area exhibited the same values. Therefore, the parameters to be inverted were the Kelvin shear modulus, Kelvin viscosity coefficient, protolith Maxwell viscosity coefficient, and Maxwell viscosity coefficient of the support and reinforcement area, and the numerical values obtained through this inversion are listed in Table 3.

By substituting the parameters shown in Table 3 into the numerical calculation, a comparison between the displacement calculation curve and monitoring curve at the monitoring location was obtained, as shown in Fig. 13. The existence of a strong coincidence is evident, which meant that the mechanics model and parameters used for the calculation were more effective in describing the rheological mechanical behavior of the surrounding rock in the chlorite schist tunnel section and could be used as a basis to analyze the structural safety of the surrounding rock and lining during the operational period.

5. Safety analysis and assessment of the surrounding rock and lining structure

The deformation rate of the rocks surrounding the highly squeezed and deformed chlorite schist section of the tunnel could be well controlled after its excavation, support installation, and reinforcement. The rate could be lowered to less than 0.2 mm/d, which met the pouring condition of the lining. Following the lining's completion, water's temporal connection through tunnel was lost and the lining was only subjected to deformation pressure from the surrounding rocks. Water penetrated into surrounding rocks when connected through tunnel, causing changes in the pore pressure of the surrounding rock and influencing the size of the effective stress, which led to the deformation development of the surrounding rock. The infiltration of internal water was followed by wetting-induced softening of the surrounding rock to a certain extent, and the mechanical parameters of rock mass were decreased. This caused high pressure to be exerted on the lining, which influenced the long-term operational safety. During this process, due to the fact that the chlorite schist belonged to the water-resisting layer and had an extremely low permeability, and that the external water was not exposed during the excavation, the minimal external water effect was not worthy of consideration for the study.

In accordance with the aforesaid actual engineering conditions, and on the basis of the rheological mechanics model of the rock mass, which were selected in the preceding section of this study, as well as the mechanical parameters of the surrounding rock obtained through the inversion, the simulation of the excavation, support, and reinforced support processes of the seriously squeezed deformation tunnel section of the chlorite schist is discussed in the following section. Here, the numerical model and calculation condition are the same as in Section 4.2. Therefore, based on the design scheme for the lining structure, the stress conditions of the lining during the initial period after the completion of the lining pouring, and under the conditions of long-term internal water infiltration and rock softening conditions, were simulated.

In accordance with the design scheme for the lining, the vault and

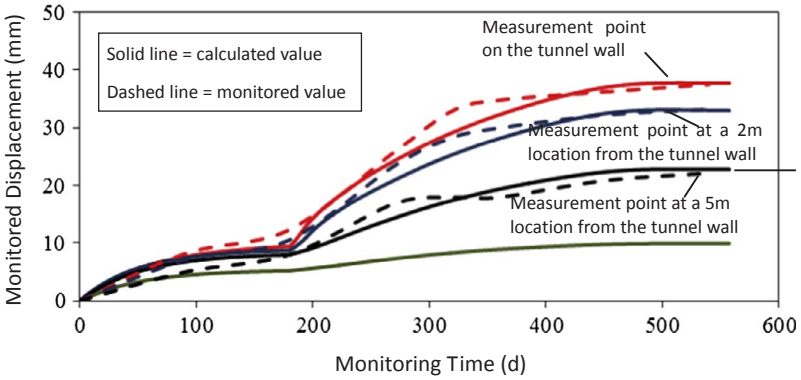

Fig. 13. Comparison between the calculated displacement curve and actual measured displacement curve at the monitoring location.

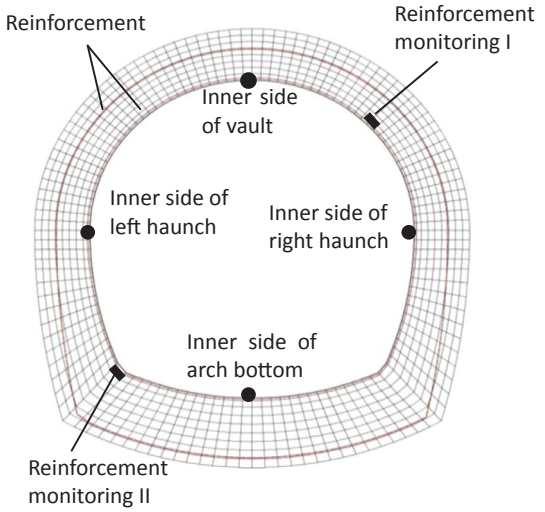

Fig. 14. Schematic diagram of the lining calculation monitoring positions.

Table 4
Mechanical parameter values of the concrete and reinforcements.

	Elasticity modulus E (GPa)	Poisson's ratio	Cohesive force c (MPa)	Internal friction angle ϕ (°)	Cross-sectional area (cm^2)
Concrete lining	28.0	0.3	2.73	54.4	–
Reinforcement	200	–	–	–	32.15

side (left & right) haunches' thicknesses were 1.8 m, and the arch bottom thickness was 2.4 m. During the calculation, the concrete lining adopted a solid unit simulation, while the concrete internal reinforcement adopted a cable unit simulation, as shown in Fig. 14. The simulation of the concrete adopted a Mohr-Coulomb model, while the reinforcement simulation adopted a linear elastic model, with its mechanical parameters shown in Table 4.

After the initial mechanical analysis, it was determined that the adverse location of the reinforcement stress in the lining was mainly located at the right spandrel and left skewback locations near the inner wall of the lining. Therefore, monitoring points were arranged at these two positions. For example, reinforcement monitoring I and reinforcement monitoring II were set in place, as shown in Fig. 14. Meanwhile, in order to better understand the stress state of the two reinforcement monitoring positions, the maximum and minimum principal stresses of the lining at these positions were monitored. In addition, this study also arranged four tangential stress monitoring points for the lining at the left and right haunches, vault, and arch bottom, as shown in Fig. 14.

5.1. Stress status during the early period after the completion of the lining pouring

This section analyses the status of the stresses in the lining after completion of the tunnel excavation and installation of the bottom support and before its opening for the operations. The stress evolution curves for the four monitoring locations (left and right haunches, vault, and inner side of the arch bottom) of the lining were obtained through calculation, as shown in Fig. 15. It can be seen that, after the lining construction was completed, the deformation pressure resulting from the rheology of the surrounding rocks caused the lining to gradually generate stress. In addition, the tangential stress at the monitoring location gradually decreased over time, and the initial decrease rate was high. With the increase in the supporting force of the lining to the surrounding rock, the rheological deformation of the surrounding rock became constrained. At that point, the change rate of the tangential

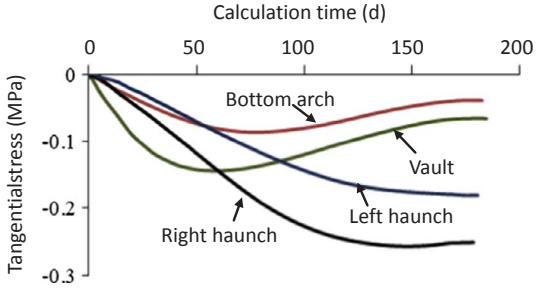

Fig. 15. Curve of the changes in the calculated tangential stress value at the inner side of the lining over time. *Note:* For the lining stresses in the figure, the negative values represent the pressure stress, while the positive values represent the tensile stress.

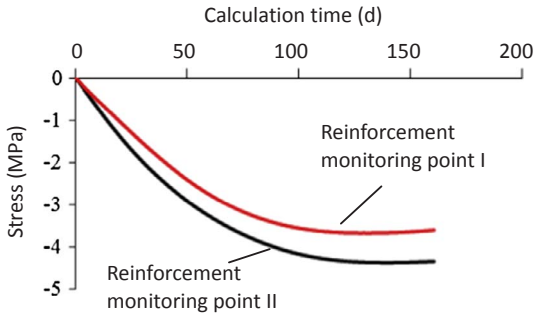

Fig. 16. Curve representing the changes in the reinforcement stress at the inner side of the lining over time. *Note:* All of the reinforcement stresses shown in the figure are the pressure stresses.

stress of the lining decreased and then began to converge on the 160th day following the completion of the tunnel's lining construction. The tangential stress at the inner side of the bottom arch was approximately −0.039 MPa; the tangential stress at the inner side of vault was approximately −0.066 MPa; the tangential stress at the inner side of the left haunch was approximately −0.18 MPa; and the tangential stress at the inner side of the right haunch was approximately −0.25 MPa.

The calculated stress curves for the reinforcement monitoring points I and II are shown in Fig. 16. It can be seen in the figure that the stress value of the reinforcement gradually decreased with the increase in the deformation pressure, which resulted from the rheology of the surrounding rock after the completion of the lining. At the beginning, the decrease rate of the reinforcement stress was larger, which then decreased rapidly over time. The reinforcement stress value of monitoring point I started to converge after the tunnel lining had been completed for approximately 160 days and then stabilized at approximately −3.62 MPa. The reinforcement stress value of monitoring point II started to converge after the tunnel lining pouring had been completed for approximately 160 days and stabilized at approximately −4.36 MPa.

Fig. 17 shows the lining's maximum and minimum principal stresses

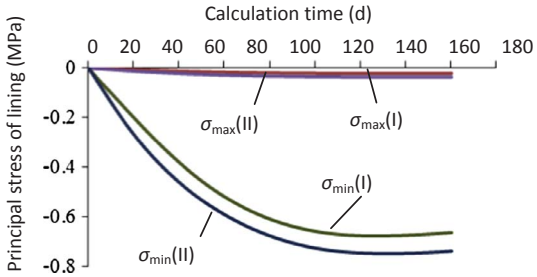

Fig. 17. Curve representing the principal stress at the reinforcement monitoring locations. *Note:* For the lining stress in the figure, the negative values represent the pressure stress, while the positive values represent the tensile stress.

change curve at the reinforcement monitoring positions. It can be seen that, after the lining construction was completed, the stress value of the lining decreased over time and finally became stable. When the tunnel lining construction had been completed for approximately 160 days, the maximum pressure stress of the lining at monitoring point I stabilized to approximately −0.66 MPa. When the tunnel lining construction had been completed for approximately 200 days, the maximum pressure stress value of the lining at monitoring point II stabilized at approximately −0.74 MPa.

As detailed above, it was determined that within a short period following the completion of the lining construction, the internal water did not intrude into the surrounding rock and did not lead to the softening of the surrounding rock. The creep deformation of the surrounding rock basically converged, due to the constraint of the lining. The maximum principal stress, minimum principal stress, and reinforcement stress inside the lining were determined to be low, and the safety of the lining was very good.

5.2. Lining safety analysis under the condition of long-term inside-to-outside seepage

In this study, the analysis of the safety of the lining under the condition of long-term inside-to-outside seepage included the analysis of the surrounding rock, lining, and internal water, as well as their interaction. Therefore, this was characterized as a fluid-solid coupling issue. An important mechanical characteristic of fluid-solid coupling is the fluid-solid interaction. In our case, it meant that the effective stress of the tunnel's surrounding rock changed due to the changes in the pore pressure distribution, which subsequently led to the deformation of the surrounding rock. This deformation along with the disturbances in the stress field produced changes in pore pressure distribution. This interaction continued until a balance was reached.

An isotropic seepage model was used for the calculation of the seepage field. The seepage coefficient of the chlorite schist protolith was 9e−6 cm/s, and the seepage coefficient of the consolidated area after grouting was 1e−5 cm/s, according to the water pressure test results. In addition, the seepage coefficient of the concrete lining was 1e−5 cm/s. The fluid modulus was 2e8 Pa and the porosity of the chlorite schist protolith was 0.3 (Zhang et al., 2016).

In order to simulate the inside-to-outside seepage circumstances in the tunnel, a 38-m fixed water head was added to the internal boundary of the tunnel, and the permeable boundary conditions were set on the peripheral boundary. Meanwhile, after considering the action of gravity, the distribution law of the pore water pressure, which was obtained under the condition of long-term inside-to-outside seepage, was determined and is shown in Fig. 18. It can be seen from the figure that 0.35 MPa of pore water pressure was generated around the tunnel lining under the long-term inside-to-outside seepage effect, and a 0.45-MPa relative pore water pressure zone was generated at a location approximately 10 m below the arch bottom due to the action of gravity.

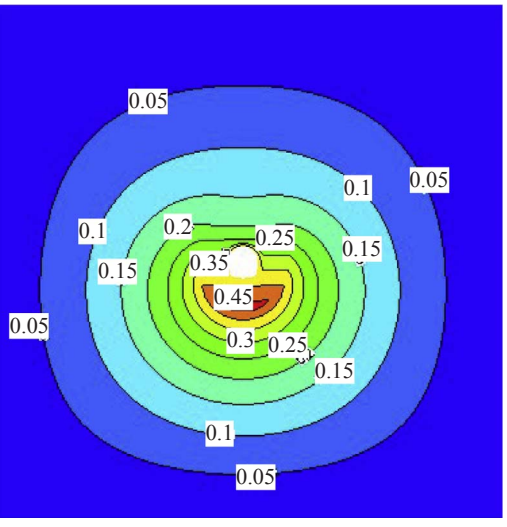

Fig. 18. Water pressure distribution under the condition of long-term inside-to-outside seepage. *Note:* For the lining stresses in the figure, the negative values represent the pressure stress, while the positive values represent the tensile stress.

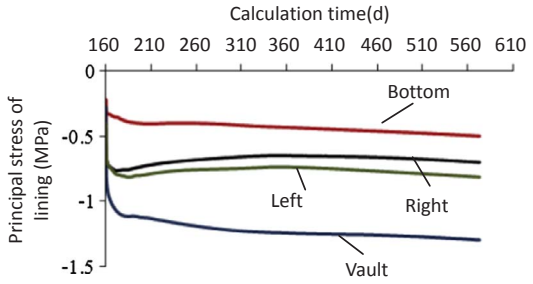

Fig. 19. Curve representing the changes in the calculated lining stress value over time under the condition of inside-to-outside seepage.

Fig. 19 shows the calculated stress evolution curve of the lining. It can be seen from the figure that a certain pore water pressure formed in the surrounding rock and lining of the tunnel, due to the impact of the inside-to-outside seepage following the headrace tunnel was being put into normal operation. This led to a re-adjustment of stress in the surrounding rock and lining. The tangential stresses at the four monitoring points of the lining were significantly changed compared with those before the operation. In addition, the stress value became stable after the headrace tunnel was put into normal operation for approximately 250 days. During this time, the tangential pressure stress at the inner side of the arch bottom decreased by nearly 0.46 MPa (compared with that of the pre-operation) and gradually stabilized at approximately −0.50 MPa. The tangential pressure stress at the inner side of the vault decreased by almost 1.23 MPa (compared with that of the pre-operational) and then gradually stabilized at approximately −1.30 MPa. The tangential pressure stress at the inner side of the left haunch decreased by nearly 0.63 MPa (compared with that of the pre-operational) and gradually stabilized at approximately −0.81 MPa. The tangential pressure stress at the inner side of the right haunch decreased by nearly 0.45 MPa (compared with that of the pre-operational) and gradually stabilized at approximately −0.70 MPa.

Fig. 20 shows the curve for the calculated reinforcement stresses of monitoring points I and II. It can be observed from the figure that, during the operational period of the headrace tunnel, the reinforcement stress value at monitoring point I and II gradually stabilized to approximately −8.40 MPa respectively after the tunnel lining construction was completed, for duration of approximately 250 days, under the effects of inside-to-outside seepage. The post-lining, reinforcement stress values were obviously changed as compared to per-lining values due to the added pore water pressure.

Fig. 21 shows the curve for the calculation principal stress of the

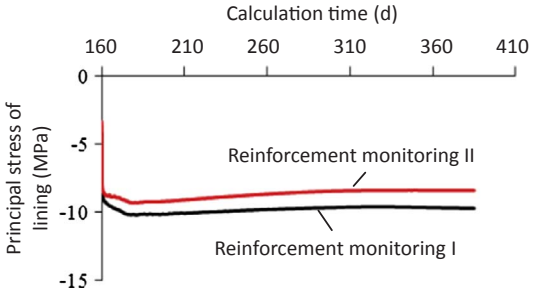

Fig. 20. Curve representing the change of the calculated reinforcement stress value over time under the inside-to-outside seepage condition. *Note:* All of the reinforcement stresses shown in the figure are the pressure stresses.

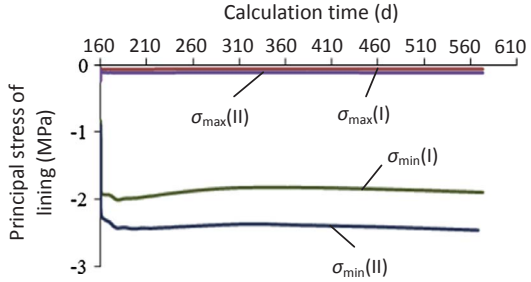

Fig. 21. Curve representing the calculated lining stress at the reinforcement monitoring locations. *Note:* For the lining stress in the figure, the negative values represent the pressure stress, while the positive values represent the tensile stress.

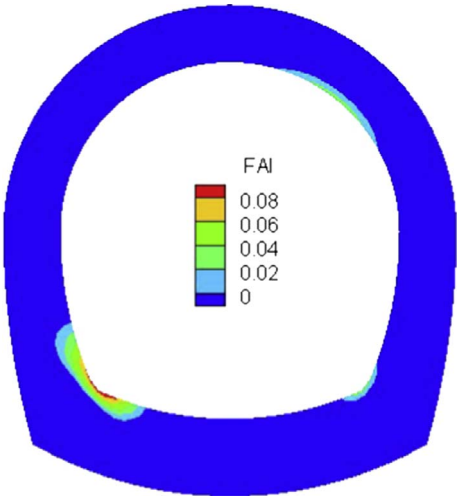

Fig. 22. Contour map for the FAI values inside the lining.

lining at the reinforcement monitoring locations. It can be seen from the figure that the minimum principal stress value of the lining at monitoring point I gradually stabilized to approximately −1.83 MPa when the tunnel lining construction was completed, for approximately 250 days. The minimum principal stress value of the lining at monitoring point II gradually stabilized at approximately −2.43 MPa when the tunnel lining construction was completed, for approximately 250 days.

In accordance with the failure approach index (FAI) distribution of the lining shown in Fig. 22, all of the FAI values of the lining were positive. In addition, the maximum FAI value was only 0.08, far lower than 1.0, which meant that the lining structure was far from reaching the yield. In other words, the lining structure had a very high safety degree.

It can be known from the above analysis that the lining structure of the headrace tunnel had a very high safety level under the fluid-solid coupling effect of the inside-to-outside seepage.

5.3. Safety analysis of the lining and surrounding rock with consideration of the softening of the rock mass under the conditions of inside-to-outside seepage

After making contact with the water, the elasticity and strength parameters of the chlorite schist decreased to some extent. During project's operational period, the reinforced concrete lining had no drainage hole, and the surrounding rock had been plugged by grouting. However, the inside-to-outside seepage problem inevitably appeared due to the fact that the lining and rock mass in the grouting circle had a certain degree of permeability. Considering the project's life span it was highly necessary to consider the cases of the softening of surrounding rocks. Relatively speaking, the lining and surrounding rock had a lower permeability and little water intrusion, hence low water percolation

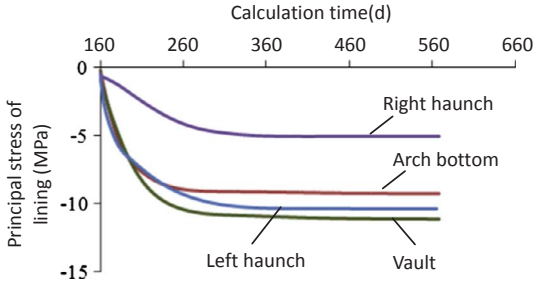

Fig. 23. Curve representing the changes in the monitored stress values of the lining over time after considering the wetting-induced softening. *Note:* For the lining stress in the figure, the negative values represent the pressure stress, while the positive values represent the tensile stress.

speeds. Therefore, the actual softening degree of the surrounding rock was lower than that shown in the laboratory saturation testing. However, it was difficult to obtain the quantitative relationship. In this study, the reduction coefficient of the calculation parameters was obtained in the laboratory as per suggestions reached upon by the comprehensive geological survey. The conservatively considered part was used as the safety reserve or to deal with the large variability problem of the mechanical property of the chlorite schist. As can be seen in Fig. 18, the inside-to-outside seepage mainly occurred in the reinforcement area, and the protolith had very poor permeability. Therefore, in this study, the softening problem was not considered in the protolith. Through integrating the test results and the mechanical response analysis results of the surrounding rock in situ, the strength parameter of the consolidated area was found to be reduced by 30%. In addition, the elasticity modulus was reduced by 80% after the inside-to-outside seepage led to the softening of the surrounding rock.

As it was difficult to determine the actual timeframe of the inside-to-outside seepage and softening of the surrounding rock, this analysis considered the softening of the rock mass on the basis of the calculation results in the initial period after the completion of the lining pouring. This resulted in a difference from the actual response time of the surrounding rock and lining. However, it had no impact on the evaluation of the lining safety.

Fig. 23 shows the curves for the tangential stresses of the lining at the four monitoring positions: inner side of the tunnel vault, inner side of the bottom arch, and inner sides of the left and right haunches. It can be seen that the stress values of the lining at each monitoring point, were clearly changed when wetting-induced softening of the surrounding rocks was taken into account as compared to when it was not given any weightage. The tangential stresses of the lining were obviously decreased and became stable 300 days after the convergence of the steady rheological deformation. During this time, the tangential pressure stress at the inner side of the bottom arch was reduced by approximately 8.79 MPa (compared with not considering the softening of the rock mass) and gradually stabilized at approximately −9.29 MPa. The tangential pressure stress at the inner side of vault was reduced by approximately 9.87 MPa and gradually stabilized at approximately −11.16 MPa. The tangential pressure stress at the inner side of left haunch was reduced by approximately 9.60 MPa and gradually stabilized at approximately −10.41 MPa. The tangential pressure stress at the inner side of the right haunch was reduced by nearly 4.37 MPa and gradually stabilized at approximately −5.07 MPa.

Fig. 24 shows the reinforcement stress status at monitoring points I and II. It can be seen from the figure that after the seepage became stable and the rheological deformation convergence has been completed for approximately 300 days the reinforcement stress value at monitoring point I and II gradually stabilized at approximately −55.2 MPa and −60.28 MPa respectively.

Fig. 25 shows the curves for the changes in the maximum and minimum principal stresses of the lining at monitoring points I and II. It can be seen from the figure that the maximum pressure stress value of

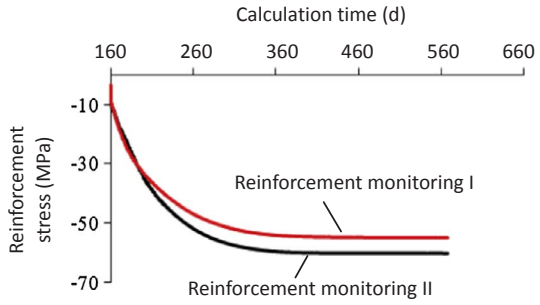

Fig. 24. Curve representing the changes in the monitored reinforcement stress values over time after considering the wetting-induced softening. *Note:* All of the reinforcement stresses shown in the figure are the pressure stresses.

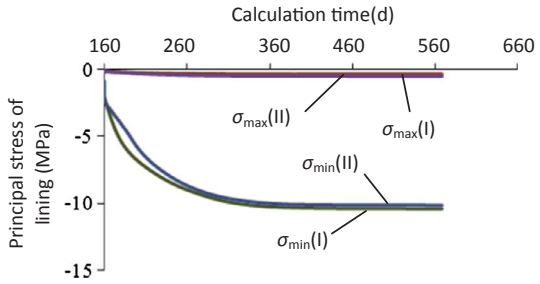

Fig. 25. Monitoring curve for the lining stresses at the reinforcement monitoring locations after considering the wetting-induced softening. *Note:* For the lining stresses in the figure, the negative values represent the pressure stress, while the positive values represent the tensile stress.

the lining at monitoring point I gradually stabilized at approximately −10.41 MPa after the seepage became stable and the rheological deformation convergence had been completed for approximately 300 days. The maximum pressure stress value of the lining at monitoring point II gradually stabilized at approximately −10.14 MPa.

Fig. 26 shows the FAI distribution in the lining. It can be seen from this figure that all of the FAI values of the lining were positive. The maximum value was 0.45, which was much lower than 1.0. In other words, the lining structure did not enter the yield state, which meant that the lining was still within the safety scope.

From the above analysis, the lining structure still maintained a better safety rate after simultaneously considering the elasto-plastic deformation, rheological deformation, and the inside-to-outside seepage of the surrounding rock in the headrace tunnel during its operational period, as well as the responses resulting from the interaction between the pore pressure and stress, the wetting-induced softening of the surrounding rock, and so on. Therefore, these results confirmed that the current lining design scheme as being reasonable.

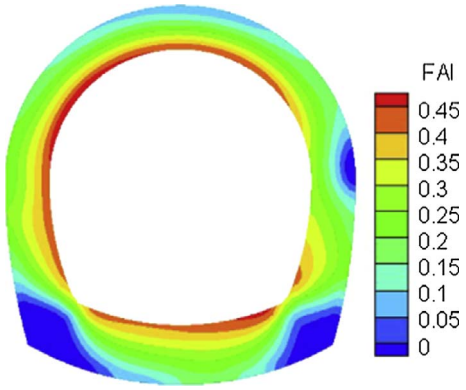

Fig. 26. Contour map for the FAI values of the lining after considering the wetting-induced softening.

6. Concluding remarks

During the construction of deep-buried long tunnels under the conditions of high-stress and soft rock environments, the stability of the tunnel construction is a formidable issue that needs to be highlighted. The chlorite schist tunnel section in the headrace tunnel of the Jinping II Hydropower Station had a buried depth of 1550–1850 m and a gravity stress between 42 and 50 MPa. During the construction, the tunnel encountered serious large deformations, and even collapsing problems, which posed extremely large threats to the stability of structure's lining.

Due to excessive deformation in the surroundings rocks where the tunnel continued through chlorite schist, this study conducted a detailed examination of the concerned rock units for engineering geological conditions and the circumstances leading to squeezing deformation following the excavation of upper bench. It also thoroughly examined the prevailing conditions of the initial support and circumstances for support reinforcement of the surroundings rocks following the expansion of the excavation in the chlorite schist section.

Then, this study examined the engineering mechanical properties of the chlorite schist through laboratory testing and on-site monitoring. It was concluded that the deformation and strength characteristics of the chlorite schist in the Jinping II Hydropower Station displayed obvious wetting-induced softening effects, while the confining pressure had a positive effect of inhibiting the softening effect of the surrounding rock.

Meanwhile, the rheological characteristics of the chlorite schist were found to be greatly influenced by the stress levels. When the stress level was low, the rheological characteristics were not obvious. However, when the stress level was high, the rheological characteristics became very obvious. Considering this, the CVISC model is adopted to describe the rheological mechanics behavior of the chlorite schist. The displacement back analysis method based on PSO was used to invert the calculation parameters of the model.

Finally, the rheological mechanics model was adopted to analyze the lining stress circumstances of the tunnel during the initial period following the completion of the lining, as well as the entire process from construction to operation, under the conditions of long-term inside-to-outside seepage and softening of the rock mass. During the initial period, the internal water did not intrude into the surrounding rock. The calculation results showed that, after the lining pouring had been completed for approximately 160 days, the creep deformation of the surrounding rock basically converged. The maximum and minimum principal stresses in the lining, as well as the reinforcement stress, were determined to be low, and the lining displayed good safety characteristics. In instances, where long-term inside-to-outside seepage was involved, the maximum and minimum principal stresses in the lining as well as the reinforcement stresses, gradually stabilized at low values after the tunnel lining construction had been completed for 250 days. In addition, the lining structure of the headrace tunnel displayed a high degree of safety under the fluid-solid coupling effects of the inside-to-outside seepage during the operational period. Considering the instances where wetting-induced softening of chlorite schist was involved during the operation life span, it was concluded that lining stress was basically stable after the seepage became stable and the rheological convergence deformation had been completed for approximately 300 days. Furthermore, the lining structure still maintained a good degree of safety at that time.

The study concluded the practicality of the reinforcement design scheme in practice and also evaluated the degree of safety for the lining structures during their operation life span. The research results played an important role in guiding the project designs and construction. Furthermore, the results can provide important references for the designing of supports for future deep-buried soft rock engineering projects.

Acknowledgements

This research was supported by The National Program on Key Basic Research Project of China [Grant No. 2014CB046902], the National Science Foundation of China [Grant No. 41172288], [Grant No. 51427803], [Grant No. 51279201] and [Grant No. 51404240]. The work in this paper was also supported by funding from the Youth Innovation Promotion Association CAS.

References

Bonini, M., Debernardi, D., Barla, M., Barla, G., 2009. The mechanical behaviour of clay shales and implications on the design of tunnels. Rock Mech. Rock Eng. 361–388.

Carranza, T.C., Diederichs, M., 2009. Mechanical analysis of circular liners with particular reference to composite supports. For example, liners consisting of shotcrete and steel sets. Tunn. Undergr. Space Technol. 24, 506–532.

Fahimifar, A., Monshizadeh Tehrani, F., Hedayat, A., Vakilzadeh, A., 2010. Analytical solution for the excavation of circular tunnels in a visco-elastic Burger's material under hydrostatic stress field. Tunn. Undergr. Space Technol. 25, 297–304.

Feng, X.T., Zhang, C.Q., Qiu, S.L., Zhou, H., Jiang, Q., Li, S.J., 2016. Dynamic design method for deep hard rock tunnels and its application. J. Rock Mech. Geotech. Eng. 8 (4), 443–461.

Guan, Z., Jiang, Y., Tanabashi, Y., Huang, H., 2008. A new rheological model and its application in mountain tunneling. Tunn. Undergr. Space Technol. 23, 292–299.

He, M.C., Leal e Sousa, R., Müller, André, Vargas Jr., Eurípedes, Ribeiro e Sousa, L., Chen, X., 2015. Analysis of excessive deformations in tunnels for safety evaluation. Tunn. Undergr. Space Technol. 45, 190–202.

Lian, G.W., Hai, L.L., Jian, Z., 2008. Numerical simulation of creep characteristics of soft roadway with bolt-grouting support. J. Central South Univ. Technol. 15, 391–396.

Liao, H.J., Pu, W.C., Qing, W.C., 2006. Study on softening constitutive model of diatomaceous soft rock based on strain space. Chin. J. Rock Mechan. Eng. 27 (11), 1861–1866 (in Chinese).

Liu, N., Zhang, C.Q., Chu, W.J., Zhu, H.C., Zhang, W., Zhang, Y., 2013. Deformation behavior and stability analysis of deep chlorite schist. Chin. J. Rock Mechan. Eng. 32 (10), 2045–2052 (in Chinese).

Ministry of Housing and Urban-Rural Development of the People's Republic of China, 2015. GB/T50218-2014 Standard for engineering classification of rock masses. China Planning Press, Beijing.

Ministry of Water Resources of the People's Republic of China, 2008. GB 50487–2008 Code for Engineering Geological Investigation of Water Resources and Hydropower. China Planning Press, Beijing (in Chinese).

Pellet, F.L., 2009. Contact between a tunnel lining and a damage-susceptible viscoplastic medium. Comput. Model. Eng. Sci. 52 (3), 279–296.

Pellet, F., Roosefid, M., Deleruyelle, F., 2009. On the 3D numerical modelling of the time-dependent development of the damage zone around underground galleries during and after excavation. Tunn. Undergr. Space Technol. 24, 665–674.

Sakurai, S., 1978. Approximate time-dependent analysis of tunnel supports structure considering progress of tunnel face. Int. J. Numer. Anal. Methods Geomech. 2, 159–175.

Sharifzadeh, M., Tarifard, A., Moridi, M.A., 2013. Time-dependent behavior of tunnel lining in weak rock mass based on displacement back analysis method. Tunn. Undergr. Space Technol. 38, 348–356.

Sulem, J., Panet, M., Guenot, A., 1987. An analytical solution for time-dependent displacements in circular tunnel. Int. J. Rock Mech. Min. Sci. 24 (3), 155–164.

Tang, S.B., Tang, C.A., 2012. Numerical studies on tunnel floor heave in swelling ground under humid conditions. Int. J. Rock Mech. Min. Sci. 55, 139–150.

Yoshida, N., Nishil, M., Kitamural, M., Adachi, T., 1997. Analysis of mudstone deterioration and its effect on tunnel performance. Int. J. Rock Mech. Min. Sci. 34, 3–4.

Zarei, H.R., Uromeihy, A., Sharifzadehc, M., 2012. Identifying geological hazards related to tunneling in carbonate karstic rocks – Zagros, Iran. Arab. J. Geosci. 5 (3), 457–464. http://dx.doi.org/10.1007/s12517-010-0218-y.

Zarei, H.R., Uromeihy, A., Sharifzadehc, M., 2013. A new tunnel inflow classification (TIC) system through sedimentary rock masses. Tunn. Undergr. Space Technol. 34 (1), 1–12. http://dx.doi.org/10.1016/j.tust.2012.09.005.

Zhang, C.Q., Zhou, H., Feng, X.T., 2011. An Index for estimating the stability of brittle surrounding rock mass — FAI and its engineering application. Rock Mech. Rock Eng. 44, 401–414.

Zhang, C.S., Liu, N., Chu, W.J., 2016. Key technologies and risk management of deep tunnel construction at Jinping II hydropower station. J. Rock Mech. Geotech. Eng. 8 (4), 499–512.

Zhao, K., Bonini, M., Debernardi, D., Janutolo, M., Barla, G., Chen, G.X., 2015. Computational modelling of the mechanised excavation of deep tunnels in weak rock. Comput. Geotech. 66, 158–171.

Zhou, H., Zhang, C.Q., Li, Z., Hu, D.W., Hou, J., 2014. Analysis of mechanical behavior of soft rocks and stability control in deep tunnels. J. Rock Mech. Geotech. Eng. 6, 219–226.